Marugán-Cruz, C., Serrano, D., Gómez-Hernández, J. & Sánchez-Delgado, S. (2019). Solar multiple optimization of a DSG linear Fresnel power plant. *Energy Conversion and Management*, vol. 184, pp. 571–580.

DOI: 10.1016/j.enconman.2019.01.054

Solar multiple optimization of a DSG Linear Fresnel power plant

Carolina Marugán-Cruz[a,*], D. Serrano[a], J. Gómez-Hernández[a], S. Sánchez-Delgado[a]

[a]*Energy System Engineering Group (ISE). Department of Thermal and Fluids Engineering. Universidad Carlos III de Madrid, Spain*

Abstract

Linear Fresnel power plants are currently one of the most promising concentrating solar power plants, however there are only a few commercial projects. These power plants have lower efficiency than parabolic trough collectors plants and are still expensive. To increase the efficiency of these plants the utilization of water/steam in the receivers (direct steam generation, DSG) and thermal storage (TES) has been considered.

As case-study, a 50 MW_e solar-only linear Fresnel power plant located at Seville, Spain has been considered. The effects of the solar field size as well as, the thermal storage size, on the annual production of the plant have been analyzed: Nine different solar field sizes and up to eight thermal storage sizes have been compared.

An economic optimization is presented in order to determine which plant has lowest Levelized Cost of Electricity (LCOE). It has been found that for the power plants with no-storage the optimum solar multiple (SM)

*Corresponding author

Email address: `cmarugan@ing.uc3m.es` (Carolina Marugán-Cruz)

is 1.7, whereas for the cases with thermal storage, the optimum configuration is a larger solar field (SM= 2), with a thermal storage of 2 hours.
Keywords: Solar multiple, Lineal Fresnel, Thermal Storage, Levelized Cost of Electricity

---

Nomenclarture

Abbreviations

CSP: Concentrated Solar Power

CRF: Capital recovery Factor (-)

DNI: Direct normal irradiance (W/m^2)

DSG: Direct Steam Generation

IAM: Incidence Angle Modifier

IRR: Internal Rate of Return

LCOE: Levelized Cost of Electricity [c€/kWh_e]

LFR: Linear Fresnel Reflector

PCM: Phase Change Materials

PTC: Parabolic Trough Collector

TNPV: Total Net Present Value

SM: Solar Multiple

SPT: Solar Power Tower

TES: Thermal Energy Storage

Symbols

A: Area [m^2]

Ap: Aperture area [m^2]

B_k: Annual revenue [€]

C_{invest}: Investment cost [€/kW$_{\mathrm{e}}$]

C_k: Annual expenses [€]

$C_{O\&M}$: Operation and maintenance costs [€/kW$_{\mathrm{e}}$]

E_{ann}: Annual energy yield [GWh]

$f_{ins,ann}$: Annual insurance cost [%]

H_{rc}: Receiver height above primary reflector [m]

IC: Investment costs [€]

i_{rate}: Debt interest rate [%]

K: Correction factor

L: Length [m]

$\dot{m}$: mass flow rate of steam $[kg/s]$

n: Service period $[years]$

N: Number

P: Pressure [Pa]

q_{pipes}: Piping thermal losses $[W/m^2]$

$\dot{Q}$: Thermal power [kW$_{\mathrm{t}}$h]

r: Interest rate of the loans [%]

RY: Repayment period $[year]$

ST: Local Solar Time $[h]$

T: Temperature $[^{\circ}C]$

$\dot{W}$: Power of the cycle [MW$_{\mathrm{e}}$]

Greek letters

α: Solar altitude angle [rad]

γ: Solar azimuth angle [rad]

η: efficiency

θ: Incident angle [rad]

τ: Discount rate [%]

Subindex

amb: ambient

ave: average cu: control unit

e-m: electro-mechanical

end: end losses

inc: incident

l: longitudinal

loop: collector loops or rows

mir: mirrors

PB: power block

off: off-design conditions

ref: reference conditions

SF: solar field

shad: shaded

T: turbine

Tot: total solar field

t: traverse

0: optical

1. Introduction

Reducing the green gas emissions comes along with reducing the dependence on fossil fuels and the deployment of renewable energies, but new technologies must compete on cost with the more classic energy sources. Concentrated solar technology can be used to generate electricity either: by using solar energy as the only resource to power a Rankine cycle (Mills, 2004) or by hybridating solar energy with conventional power-plants (Yang et al. (2011); Li et al. (2017); Petrakopoulou et al. (2017)). Alternative uses of concentrated solar energy are heat supply for different industrial sectors (Farjana et al. (2018)) or covering refrigeration demands (Al-Alili et al. (2012)). Concentrating solar power (CSP) is an important alternative for providing clean and secure energy.

Currently there are four main technologies in CSP: solar power towers (SPT), dish Stirling, parabolic trough collectors (PTC) and linear Fresnel reflectors (LFR). Solar power towers and dish Stirling are point focus techniques while parabolic troughs and Fresnel collectors are known as line focus technologies. Among CSP techniques, parabolic trough collectors have been commercially proven more than any other, however linear Fresnel collectors are significantly less expensive and can be an alternative to PTC.

Linear Fresnel technology is composed of many long flat, or slightly curved, reflectors which focus on an elevated receiver parallel to the reflectors axis (Mills and Morrison (2000)). The receiver is typically mounted on a structure suspended above the mirror arrays (at 5 -15 m high) which does not need to be supported by the tracking device (Desai and Bandyopadhyay (2017)). The LFR technology is significantly cheaper than the parabolic trough (Barlev et al. (2011)), mainly due to the cheaper mirrors and lower structural costs. There are other important advantages such as low wind loads or lower maintenance costs that could turn this technology an alternative to parabolic troughs, despite their much lower overall efficiency (Kumar and Reddy, 2012; Morin et al., 2012).

The design of the LFR can be tailored to use in different applications depending on the temperature of the heat generation (Zhu et al. (2014)). High temperature heat is generally used to generate electricity (Mills (2004); Desai and Bandyopadhyay (2017)), whereas low - or - medium temperature heat LFR technology has been used for multiple purposes such as: building cooling (Velázquez et al. (2010); Mokhtar et al. (2010)) and heating (Mokhtar et al. (2016)), industrial process heat supply (Mokhtar et al. (2015); Pulido-Iparraguirre et al. (2019)), or post-combustion carbon-capture (Wang et al. (2017)).

Typically the fluid heated in the LFR receiver is high-pressure water (Desai and Bandyopadhyay (2017)) that can be used directly in the steam turbine in a Rankine cycle. The obvious advantage of direct steam generation (DSG) power plants is that heat exchangers are not necessary and that the energy efficiency can be higher. Recent studies have evaluated the performance of the LFR using other fluids such as molten salts (Schenk et al. (2014); Grena and Tarquini (2011); Qiu et al. (2015); Bacheller and Stieglitz (2017)), or thermal oil (Cau and D. (2014); Wang et al. (2017)). Despite the advantages of using those fluids, all commercial LFR power plants currently in operation and under development or construction use water/steam as working fluid.

The SunShot Innitiative, that funds programs for concentrating solar power deployment, has as a goal to lower the cost of CSP to 0.06$ per kWh by 2020. Since the solar field represents the major investment in these power plants (Kolb et al. (2011); Desai and Bandyopadhyay (2017)) the optimization of the size of the solar field is critical to reduce the costs of electricity. Thermal energy storage (TES) and operation strategy are other factors that affect importantly the price of electricity. Indeed, thermal storage allows to decouple the solar radiation from the electrical output and thereby can generate electricity during peak hours (Guédez et al., 2016). This dispatchability has to be taken into consideration when analyzing the viability of the solar projects (Kost et al., 2013)

To this regard, Izquierdo et al. (2010) studied the effects of the solar field size, the capacity factor and the storage capacity on the cost of electricity in parabolic troughs and molten salts tower plants. For both technologies, they noted that for each storage capacity, as the solar field increased, there was an initial reduction in the energy cost up to a minimum. Luo et al. (2017) studied the optimum solar field size for a steam generation dual-receiver solar tower with storage. They concluded that the solar field size was the sub-system that affected mostly the LCOE. Montes et al. (2009b) studied the influence of the solar field size on the annual performance of the power plant of a solar-only thermal-oil parabolic trough collector plant. Montes et al. (2009a) described the role of the solar field size on the performance of a hybrid (fossil-solar) DSG PTC power plant with thermal storage. Giostri et al. (2012) compared the effects of different heat transfer fluids (molten salt, synthetic oils and water/steam) in parabolic plants with no thermal storage, and concluded that DSG plants have higher on-design and annual average efficiency than using any other fluid. Similarly, Feldhoff et al. (2012) compared the use of DSG and oil in parabolic plants with integrated thermal storage. Morin et al. (2012) presented the costs that DSG linear Fresnel technology should have in order to be competitive with DSG Parabolic Troughs. Schenk et al. (2014) performed an energetic and economical comparison between a parabolic trough and linear Fresnel collector power plant with Solar Salt as heat transfer fluid.

Although TES technology for DSG is still immature and expensive (Feldhoff et al., 2012), significant efforts have been made for its development. Steam accumulators have been integrated with DSG tower power plants to provide energy storage for: PS10 (11 MW_e - 1 h of TES), PS20 (20 MW_e - 1 h of TES) and Khi Solar One (50 MW_e - 2 h of TES) (González-Roubaud et al., 2017). However, this TES technology, which is relatively simple and mature, presents the drawbacks of the high volume needed to store large energy quantities and the low storage temperature. Furthermore, it presents higher costs compared to molten salt TES systems for energy storages longer than 1 h (González-Roubaud et al., 2017).

The results showed the feasibility of the PCM unit for working in constant and sliding pressure modes (Laing et al., 2013). The low thermal conductivity of the PCM, which leads to slow charging and discharging rates, could be solved installing fins (Laing et al., 2012) or combining the PCM with an additive of high conductivity, such as graphite (Gil et al., 2010). In this sense, a parametric study determined the target costs of a finned PCM tank coupled to a DSG PTC power plant (Seitz et al., 2017). The PCM feasibility has been also studied in a cogeneration plant (Saarland, Germany), storing 1.5 MWh at a power level of about 6 MWth (Johnson et al., 2015, 2017). Other TES configurations for a DSG power plant of 147 MW_e combine molten salt and PCM to provide different TES capacities (Prieto et al., 2018).

More recently, (Guo et al., 2018) studied different tank configurations using liquid lead-bismuth eutectic alloy as sensible heat storage and sodium nitrate as latent heat storage. A three-tank latent heat storage system showed the highest flexibility of the TES configurations considered for a DSG PTC.

Presently, the DSG linear Fresnel plants of Zhangjiakou and Zhangbei (under development) use solid state formulated concrete units for storage (NREL, 2018).

Bellos et al. (2018) studied the daily performance of a LFR collector but to the best of our knowledge, this is the first study to present an economic optimization of the solar multiple and the thermal energy storage size for a DSG linear Fresnel power plant.

The present paper compares the annual behavior of linear Fresnel power plants with different solar field sizes and different storage capacity. A 50 MW_e linear Fresnel power plant with no thermal storage has been chosen as a reference case. The paper is structured as follows: in section 2, a description of the components and parameters of the solar power plant is presented, in section 3 the different solar field sizes and storage capacities are proposed and in section 4 the annual performance of the plant is presented together with an economical analysis. Finally the conclusions are discussed in the last section of the manuscript (section 5).

2. Solar Power Plant Description

The typical size of a solar power plant is 50 MW_e or smaller (NREL, 2018) and hence, the power block considered here is a 50 MW_e reheat regenerative Rankine cycle. Steam turbines used for CSP applications typically consist of a high pressure turbine and an intermediate / low-pressure turbine, with several extractions to preheat the steam. To prevent a large humidity fraction at the exit of the steam turbine, reheating is necessary.

A scheme of the power plant can be seen in figure 1. As was said above, two cases have been considered: with no thermal storage and with thermal storage. In the first case, when the solar thermal field is generating enough thermal energy the power block will be able to work at nominal conditions, at full load, or otherwise the power block will work at part-load conditions. If the solar power plant has thermal storage, the power block will be able to operate for longer periods and it is decoupled from the thermal energy production. The details of the operation when storage is considered are explained bellow (see 2.3).

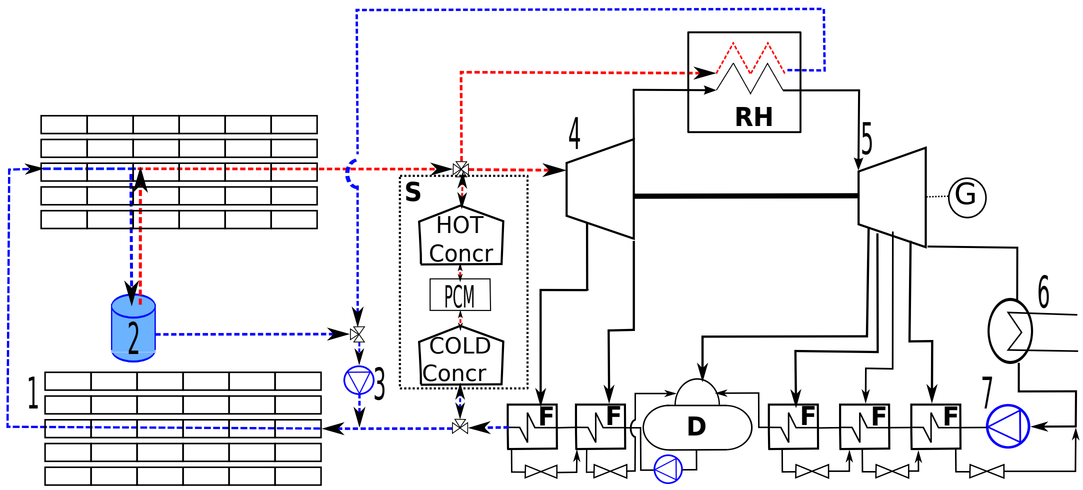

Figure 1: Simplified scheme of the linear Fresnel solar field and power plant: 1. Fresnel solar field. 2. Steam separator. 3. Recirculating solar field pump. 4. High Pressure Turbine. 5. Low Pressure Turbine. 6. Condenser. 7. Condenser pump. **RH**. Reheater. **F**. Feedwater heater. **D**. Deaerator. **S**. Storage system. **G**. Generator

2.1. Fresnel plant configuration

The main components of the Fresnel collectors are the primary mirrors that are supported by the tracking structure, the receiver, that typically consists of a vacuum absorber tube and secondary reflector, the control system for the primary reflectors tracking the sun and the foundation (see figure 2). Other designs have been proposed and are under the conceptual design stage or might have undergone the prototype phase (Abbas et al. (2012); Singh et al. (2010); Zhu et al. (2014)).

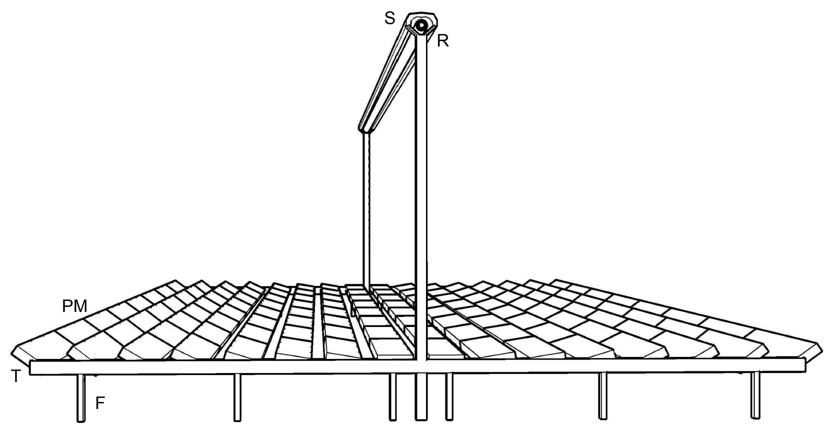

Figure 2: Control unit of a linear Fresnel Collector: F. Foundation, T: Tracking Structure, PM: Primary mirrors, S: Secondary Reflector, R: Receiver tube.

There are few linear Fresnel collectors currently being setup commercially for power production: NOVA-1, SUPERNOVA and DMS of Novatec Solar company (Novatec Solar, 2017), Industrial Solar LF-11 (Industrial Solar, 2017) or SUNCNIM (SUNCNIM, 2017). For the following study the SUPERNOVA system by Novatec Solar company has been used. This system can achieve steam temperatures up to 550 °C (Novatec Solar, 2017).

The smallest unit of the SUPERNOVA system is called control unit (see figure 2). Each control unit consists of 16 parallel rows of flat glass mirrors and each row is composed of 8 mirrors, arranged longitudinally. The parallel primary mirrors (individually tracked) focus the direct solar radiation onto the receiver located on top. The control units are arranged longitudinally to form a collector row (or loop), and each collector row has between 5 or 22 control units. The collector rows can be arranged in parallel to form a solar field. A distance of 4.5 m between each collector row is recommended. Table 1 shows the geometrical and optical parameters of these solar collectors.

Parameter	**Value**
Number of rows of mirrors per control unit	16
Number of primary mirrors per row	8
Primary mirrors width (m)	0.75
Primary mirrors length, L_{mir} (m)	5.35
Distance between mirrors in a row (m)	0.2857
Distance between rows in a control unit (m)	0.304
Aperture surface of the control unit, Ap_{cu} (m^2)	513.6
Control unit length, L_{cu} (m)	44.8
Control unit width (m)	16.56
Number of control units per collector row, N_{cu}	16
Clearance between collector rows (m)	4.5
—	—
Receiver type	Schott PTR 70
Receiver height above primary reflectors, H_{rc} (m)	7.4
Absorber outer diameter (m)	0.07
Absorber inner diameter (m)	0.065
Glass envelope outer diameter (m)	0.115
Glass envelope inner diameter (m)	0.109
Optical efficiency, η_0	0.64

Table 1: Geometrical and optical parameter of the Fresnel collectors (Lovegrove and Stein (2012); Novatec Solar (2017); Schott (2017)).

The total aperture area of the solar field, A_{SF} is calculated as:

$$A_{SF} = N_{loop} \cdot A_{loop} = N_{loop} \cdot N_{cu} \cdot Ap_{cu} \quad (1)$$

where N_{loop} is the total number of collector rows in the solar field and A_{loop} is the area of the collector row.

The solar field design chosen for this study is a recirculating field with superheating: an evaporator section and a super-heater section separated by a water-steam separator. One-through steam flow would also be possible but it is more complex to control (Wagner and Zhu, 2012).

2.2. Power block

An schematic diagram of the steam cycle is shown in figure 1. It is a regenerative Rankine cycle. Live steam pressure and temperature are chosen to be 500 °C and 112 bar (Feldhoff et al. (2012, 2010)). In the same figure it can be seen that reheating is performed between the high and low pressure turbines to reduce the humidity at the exit, so low pressure turbine inlet temperature is set to 500 °C at nominal conditions. Six regenerative water heaters are employed: two extractions from the high pressure turbine and four extractions from the low pressure turbine.

The thermal efficiency of the power block at full load (nominal conditions) is $\eta_{T,ref} = 42.41\%$ and the electro-mechanical efficiency of the generator, $\eta_{e,m}$ is 98.0%. The nominal values of the Rankine cycle are shown in table 2.

PARAMETER	VALUE
Turbine	
Inlet temperature (°C)	500
Inlet pressure (bar)	112
High pressure efficiency (%)	84
Reheat inlet temperature (°C)	500
Low pressure efficiency (%)	92
Electro-mechanical efficiency (%)	98
Extraction point pressures	
Extraction 1 (bar)	40.0
Extraction 2 (bar)	15.3
Extraction 3 (deaerator) (bar)	8.0
Extraction 4 (bar)	3.4
Extraction 5 (bar)	1.2
Extraction 6 (bar)	0.35
Pressure drop in extraction and reheating	
Extraction line 1 (%)	2.5
Extraction line 2 (%)	3
Reheating line (%)	11.75
Extraction line 3 (deaerator) (bar)	4.5
Extraction line 4 (%)	3
Extraction line 5 (%)	3
Extraction line 6 (%)	3.50
Closed feedwater heaters	
Terminal temperature difference (°C)	1.5
Drain cooling approach (°C)	5.5
Condenser	
Pressure (bar)	0.08
Condenser pump	
Isentropic efficiency (%)	75
Electro-mechanical efficiency (%)	98
Feedwater pump	
Isentropic efficiency (%)	78
Electro-mechanical efficiency (%)	98

Table 2: Nominal values of the Rankine cycle

2.3. Thermal Energy Storage (TES)

Thermal energy storage decouples energy production from solar hours and it allows a higher utilization of the power block since the extra heat produced by the solar field during the central hours can be exploited later during the day.

Different TES solutions have been evaluated for DSG, and one of the most promising is to split the system into different units depending on the water properties (Prieto et al., 2018): a preheater, an evaporator and superheater unit. For this study, the proposed TES system uses a two concrete storage modules and a phase change material (PCM) unit. Compared to other sensible heat storage types such as molten salt tanks, in this study concrete storage has been selected because it is significantly less expensive (Lovegrove and Stein, 2012; Feldhoff et al., 2012; Prieto et al., 2018).

In figure 1 a scheme of the storage subsystem can be seen, sketched inside the dotted black box (**S**). The concrete storage units together with the PCM unit can be identified in the storage subsystem.

During the charging process, the heat from the superheated steam produced in the solar field is extracted by the hot concrete unit using a heat exchanger integrated in the storage unit. At the exit of the hot concrete unit the saturated steam is introduced into the PCM that stores the latent energy from the steam as it condenses to water. The saturated water can be further cooled in the cold concrete unit. Then, the water can return to the solar field.

During the discharging process, the water coming from the power block is preheated in the cold concrete storage unit, evaporated in the PCM unit and superheated up to 480 °C in the hot concrete storage unit. During the discharging process the steam pressure at the inlet of the power block falls to 95 bar and therefore the power block efficiency is reduced. During the operation using steam from the storage the cycle operates in sliding pressure mode.

To capture the heat losses of the storage subsystem a heat loss of 5 % (Montes et al. (2009a); Prieto et al. (2018)) has been assumed for this work.

2.4. Design-point conditions

The design point of a solar power plant is commonly fixed at solar noon on the summer solstice (21st of June). The location of the solar power plant has been set at Seville, Spain. For this location the meteorological data (radiation, temperature and wind data) from the ASHRAE International Weather for Energy Calculations Version 1.1 (IWEC) has been used. The orientation of the receivers is North-South. Table 3 shows the design point conditions used for the calculations.

Parameter	Value
Collector orientation	N-S
Design point day	21 of June
Design Solar Time	12 h
Solar beam radiation (W/m^2)	850
Ambient temperature (°C)	25
Location	Seville (Spain)
Latitude	37.42 °N
Longitude	-5.9 °E
Altitude (m)	31

Table 3: Design point conditions

At design conditions the optical efficiency of the Fresnel collectors, η_0, is close to 0.65 (Novatec Solar (2017)). This parameter takes into account the receiver absorptivity, the mirrors (primary and secondary) reflectivity, the tracking errors and the fouling of mirrors and absorbers.

The incident thermal power of the field, $\dot{Q}_{inc}$, can be calculated as:

$$\dot{Q}_{inc} = \eta_0 \cdot \mathrm{IAM} \cdot \mathrm{A_{SF}} \cdot \mathrm{DNI} \tag{2}$$

where IAM is the incident angle modifier, A_{SF} is the total aperture area and DNI is the direct normal radiation. At design point the incident angle modifier has been considered one, otherwise, the incidence angle modifier can be calculated as the product of the traversal (K_t) and longitudinal (K_l) correction factors (Mertins, 2008) (see section 2.5). The shadow losses and end losses (radiation reflected by the primary mirrors that does not reach the receiver) are neglected at design conditions.

The useful thermal output of the solar field is calculated as:

$$\dot{Q}_{solar} = \dot{Q}_{inc} - \dot{Q}_{loss} - \dot{Q}_{pipes} \tag{3}$$

where $\dot{Q}_{loss}$ and $\dot{Q}_{pipes}$ are the heat losses in the solar field and pipes respectively.

To model the thermal loss of the solar receivers (PR70 Schott Advance) the experimental data from Burkholder and Kutscher (2008) has been used. The heat losses have been calculated using the following equation:

$$\dot{Q}_{loss} = a_1(T_{ave} - T_{amb})^3 + a_2(T_{ave} - T_{amb})^2 + a_3(T_{ave} - T_{amb}) \tag{4}$$

where the coefficients $a_1 = 6.779 \cdot 10^{-6}$ [W/K^3], $a_2 = -0.001823$ [W/K^2], $a_3 = 0.3207$ [W/K] have been determined using the experimental data of PR70 Schott Advance at the National Renewable Energy Laboratory (NREL) (Burkholder and Kutscher, 2008). T_{ave} is the average temperature of the fluid in the solar field, (that is the average temperature of temperature at the exit of the last feedwater heater and at the inlet of the high pressure turbine) and T_{amb} is the ambient temperature (25 °C).

The header pipes, that distribute the heat transfer fluid throughout the solar field, will also have an effect on the available heat of the Rankine cycle. To calculate the piping thermal losses of the solar field a constant value of $q_{pipes} = 0.86\ W/m^2$ has been employed. Therefore, these thermal losses depend on the solar field configuration.

2.5. *Off-design model*

The tracking system of the N-S linear Fresnel allows to track the sun to minimize the incidence solar angle on the collector surface. Nevertheless, there is an effect on the energy collected by the solar collector due to the incidence angle. This effect is the incidence angle modifier, IAM. Furthermore, under off-design conditions the performance of the solar field might diminish due to the shading between solar collectors of different rows. This effect is accounted on the shadowing efficiency, η_{shad}. Finally, the factor that takes into account the losses due to the fact that part of the radiation reflected by the mirrors does not reach the end of the receiver is called end-loss efficiency, η_{end}. Equation 5 is used to obtain the thermal energy collected by the solar field under off-design conditions:

$$\dot{Q}_{inc,off} = \eta_0 \cdot \mathrm{IAM} \cdot \eta_{\mathrm{end}} \cdot \eta_{\mathrm{shad}} \cdot \mathrm{A_{SF}} \cdot \mathrm{DNI} \tag{5}$$

As was stated above, the incidence angle modifier, IAM, can be calculated as the product of the traversal, K_t and longitudinal factors, K_l. Equations 6 and 7 have been used to calculated them (Wagner, 2012).

$$K_t = 0.9896 + 0.044 \cdot \theta_t - 0.0721 \cdot \theta_t^2 - 0.2327 \cdot \theta_t^3 \tag{6}$$

$$K_l = 1.0031 - 0.2259 \cdot \theta_l + 0.5368 \cdot \theta_l^2 - 1.6434 \cdot \theta_l^3 + 0.722 \cdot \theta_l^4 \tag{7}$$

where θ_t and θ_l are the incidence traverse and longitudinal angles respectively, that depend on the solar azimuth angle, γ, and the solar altitude angle, α (see eqs. 8 and 9) (Morin et al., 2012). Angles are expressed in rad.

$$\theta_t = \tan^{-1} \frac{|\sin(\gamma)|}{\tan(\alpha)} \tag{8}$$

$$\theta_l = \sin^{-1}(\cos(\gamma) \cdot \cos(\alpha)) \tag{9}$$

Figure 3 a shows the correction factors, K_t and K_l, with the incidence angles, and figure 3 b shows the variation of the incidence angle modifier, (IAM = $K_t \cdot K_l$) with solar time for different days of the year (22 of March, 18 of June, 21 of September and 12 of December). Due to the North-South orientation of the collectors the optical performance is slightly better in mornings and evenings than on solar noon. This effect is more important the further the day is separated from the summer solstice.

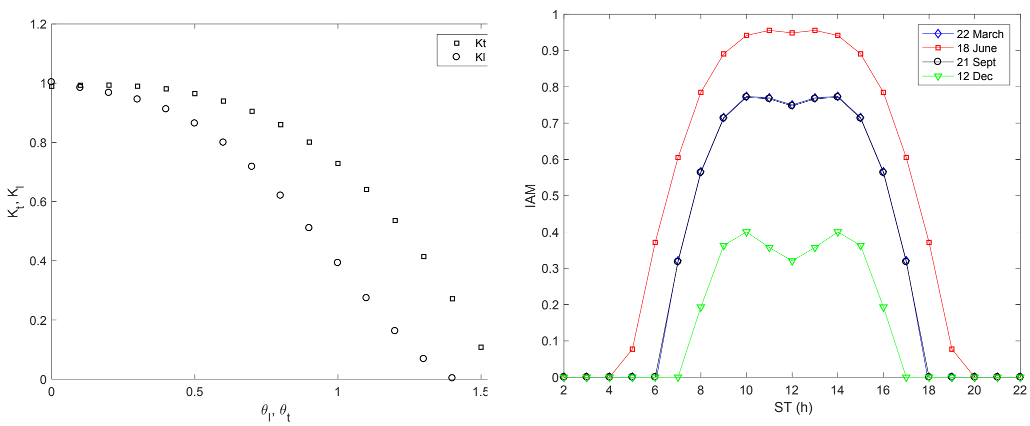

Figure 3: Optical performance of the Novatec Fresnel collector. a) Correction factors, K_t (square symbols) and K_l (circles), b) IAM for different days of the year at Seville.

It is necessary to take into account the part of the solar radiation reflected off the primary mirrors that is sent beyond the ends of the receiver and secondary reflectors (Mertins, 2008). These losses, η_{end}, depend on the longitudinal incidence angle, θ_l, the receiver height, H_{rc} and the length of the collector, L_{loop}.

$$\eta_{end} = 1 - \frac{H_{rc}}{L_{loop}} tan\left(\theta_l\right) = 1 - \frac{H_{rc}}{L_{cu} N_{cu}} tan\left(\theta_l\right) \tag{10}$$

The position of the 16 mirrors of a control unit, together with the solar incidence angle are used to determine the inclination of each mirror and to calculate the shadowing. The two-dimensional model proposed by Pino et al. (2013) has been used to calculate the inclination of the mirrors. This procedure is applied to every row and the total shaded area between rows is calculated. Finally, the shadow of the secondary reflector neighbour over the primary reflectors is taken into account. Eq. 11 describes the corresponding relation, where the shaded factor is this total shaded area, A_{shad}, and Ap_{cu} is the reflective area of the control unit.

$$\eta_{shad} = 1 - \frac{A_{shad}}{Ap_{cu}} \tag{11}$$

Finally, the hourly values of solar radiation of a "typical" year (from the ASHRAE International Weather for Energy Calculations), DNI, have been used to calculate the annual solar field energy.

2.6. *Plant Performance at Partial Load*

The gross and net output of the plant are affected by the outlet conditions of the solar field (Lippke, 1995). The steam turbine operation at part load can be controlled by 3 methods: either by controlling the steam flow rate (throttle control and governing control) or adjusting the pressure (sliding pressure method) (Polsky, 1982). The *throttle control* method reduces the steam mass flow rate by closing the "main steam stop valves", while the *governing control* regulates the steam flow rate by partially or totally closing sequentially the "steam control valves" that allow the steam into the arcs of the first stage of the high pressure turbine. Finally, in the *sliding-pressure* method (Spencer et al., 1963) the pressure at the inlet of the turbine is coupled with the pressure of the steam generator (no valves are closed) while the live steam temperature remains almost constant.

In this study, the steam turbine operation at part load is controlled by the *sliding-pressure* method. To model the thermodynamic performance of the Rankine cycle a Matlab code (Pérez-Cicala (2017)) has been used, which models the power block performance off-design using the Stodola law, as written by Patnode (2006):

$$\left(\frac{\dot{m}}{\dot{m}_{ref}}\right)^2 = \frac{P_1^2 - P_2^2}{P_{1,ref}^2 - P_{2,ref}^2} \tag{12}$$

where, $P_{1,ref}^2 - P_{2,ref}^2$ is the pressure drop over a turbine section under design conditions and $P_1^2 - P_2^2$ is the pressure drop over a turbine section at partial load. Finally, $\dot{m}$ and $\dot{m}_{ref}$ are the mass flow rate of steam at partial load and under design conditions, respectively. The turbine efficiency at part load, η_T, as a function of throttle flow ratio (the ratio of mass flow rate at part load to the mass flow rate at design conditions) has been calculated using the method of Pérez-Cicala (2017).

Furthermore, the electro-mechanical efficiency of the generator at full load is 98$\%$ (see table 2), and at partial load the efficiency of the electric generator can be found using eq. 13 (Patnode, 2006).

$$\eta_{e,m} = 0.9 + 0.258 \cdot Load - 0.3 \cdot Load^2 + 0.12 \cdot Load^3 \tag{13}$$

where $Load$ is calculated as the ratio between the turbine power and the rated turbine power.

The gross power can be calculated:

$$\dot{W}_{gross} = \eta_{e,m} \cdot \eta_T \cdot \dot{Q}_{solar} \tag{14}$$

Finally, the net power from the cycle can be found out taking into account the electric consumption of the solar field pumps, condenser pump, feed-water pump and the electrical consumption of the cooling water pump.

$$\dot{W}_{net} = \dot{W}_{gross} - \dot{W}_{Parasitic} \tag{15}$$

3. Cases studied

Nine different solar field sizes and up to eight thermal storage sizes have been studied. The size of the solar field of the different cases studied can be seen in table 4. For each solar field the capacity of storage system has been varied from 0 hours to 8 hours.

The solar multiple, SM, has been used to characterize the solar layout (Schenk et al. (2014)). The SM is defined the ratio between the solar field thermal power, $\dot{Q}_{solar}$, at design conditions and the thermal power required by the power block, $\dot{Q}_{PB,ref}$, at nominal conditions (see eq. 16). In order to achieve the nominal conditions on the power block not only instantly, the solar multiple is always greater than one in solar plants (Montes et al. (2009b)).

$$SM = \frac{\dot{Q}_{solar}}{\dot{Q}_{PB,ref}} \tag{16}$$

The thermal power required by the power block can be calculated as the ratio between the electrical power generated, $\dot{W}_{gross}$ and the efficiency of the power block at full load.

$$\dot{Q}_{PB,ref} = \frac{\dot{W}_{gross}}{\dot{\eta}_{T,ref}\eta_{e,m}} \tag{17}$$

Table 4 shows the simulation results for the solar field with different number of collector rows considered at the design point conditions for the DSG plant with no thermal storage.

Collector rows N_{loops}	Total Solar Field Area A_{TOT} (m^2)	Solar Field Aperture Area A_{SF} (m^2)	Solar Thermal Power $\dot{Q}_{solar}$ (MW$_{th}$)	Solar Multiple SM
32	$4.53 \cdot 10^5$	$2.47 \cdot 10^5$	130.54	1.03
38	$5.74 \cdot 10^5$	$3.12 \cdot 10^5$	165.36	1.31
44	$6.65 \cdot 10^5$	$3.62 \cdot 10^5$	191.47	1.51
50	$7.57 \cdot 10^5$	$4.11 \cdot 10^5$	217.57	1.72
58	$8.78 \cdot 10^5$	$4.77 \cdot 10^5$	252.39	1.99
64	$9.69 \cdot 10^5$	$5.26 \cdot 10^5$	278.50	2.20
72	$10.91 \cdot 10^5$	$5.92 \cdot 10^5$	313.31	2.47
80	$12.13 \cdot 10^5$	$6.57 \cdot 10^5$	348.12	2.75
88	$13.34 \cdot 10^5$	$7.23 \cdot 10^5$	382.93	3.02

Table 4: Summary of the simulation results at design conditions for solar plants of different solar field sizes with no storage.

4. Results and discussion

The thermal and optical model of the solar power plant operating under off-design conditions explained previously has been used to obtain the annual performance of the solar power plant with an hour timeframe.

4.1. Solar Field Performance

Figure 4 shows in combination with the DNI (right axis), the heat generated by a solar field of 32 loops ($SM = 1$) (right axis) on four representative days of the year: March 21, June 18, September 21 and December 12, using eq. 5. The days selected are clear days close to the equinoxes and solstices dates.

As could be expected, the thermal power is significantly higher on June 18, especially if compared to the thermal power obtained on December 12, since the heat obtained in the solar field is related with the IAM (see eq. 5) and the IAM is maximum in the summer solstice.

The optical performance of the collectors during the day can be observed in figure 4 too. Despite the DNI is maximum at solar noon, the thermal power generated by the solar field at solar noon is slightly smaller than right before and after it because of the IAM reduction. This effect is particularly important on December 12.

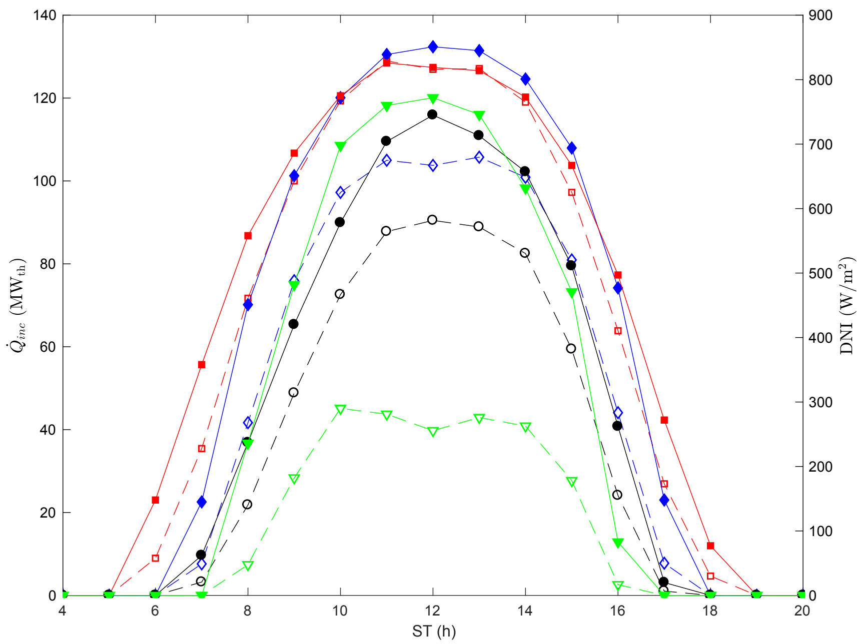

Figure 4: Direct solar radiation (right axis) and Thermal power generated (left axis) by the solar field on Mar 21 (blue ◊), June 18 (red □), Sept 21(black ○) and 12 December (green ▽). Filled symbols correspond to DNI values and empty symbols to thermal power generated by the solar field.

4.2. *Annual electricity production*

The capacity factor is the ratio of the net electricity generated, for the time considered, to the energy that could have been generated at continuous full-power operation during that period. For each solar field the maximum thermal storage has been calculated as the maximum thermal storage that increased the capacity factor, i.e the maximum thermal storage hours for the field of solar multiple of 1.99 is 6 hours, since a TES of 7 hours or bigger would give the same capacity factor of the plant.

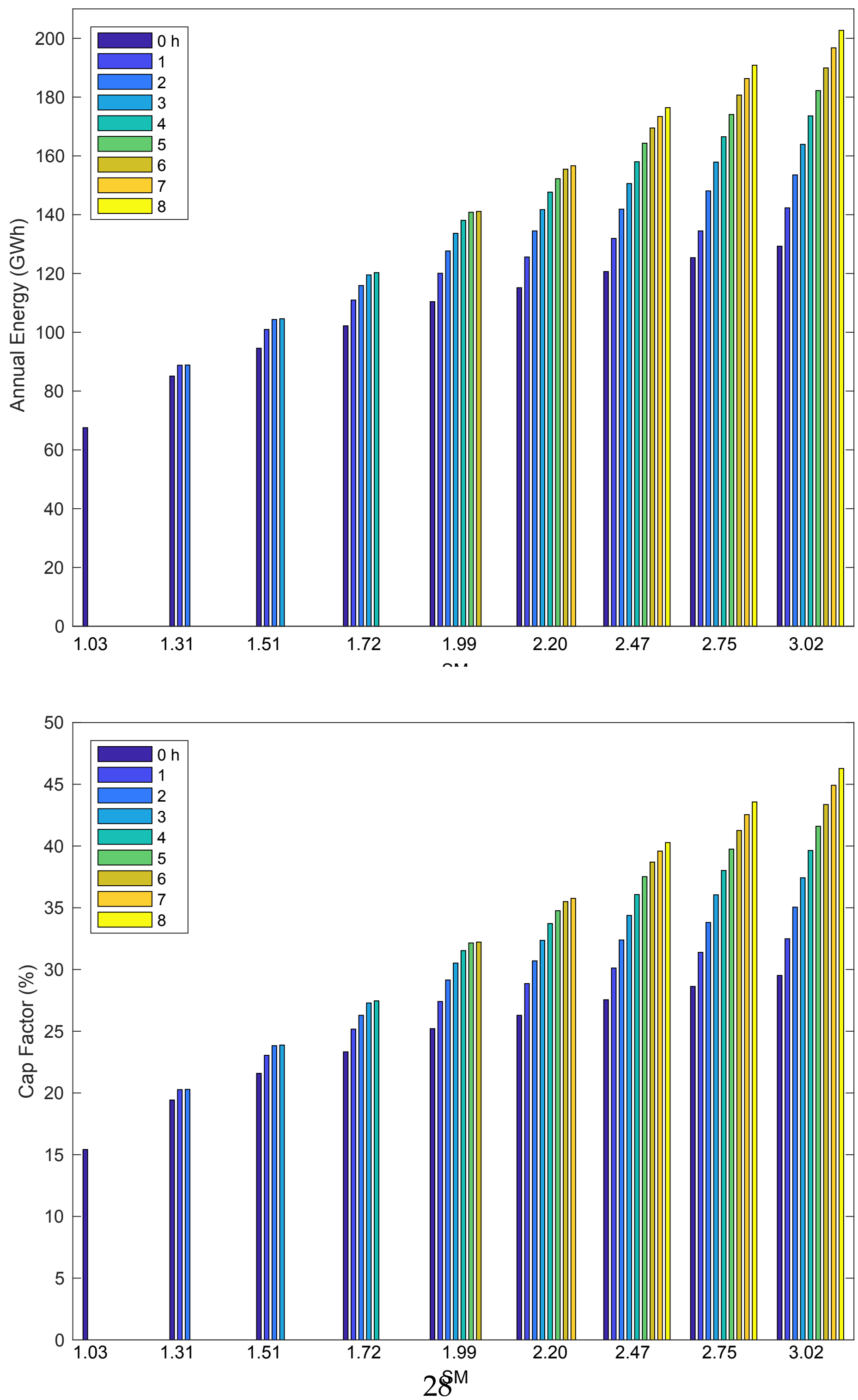

Figure 5: Summary of the annual results for different solar multiple (horizontal axis) and storage capacity (bar colors). a) Annual net electricity b) Capacity factor.

Figure 5 shows the annual electricity production (top figure) and capacity factor (bottom figure) for different solar fields sizes and different thermal storage capacities. As was expected, the annual net electricity and capacity factor increase with the solar multiple. As the size of the solar field increases, so does the solar thermal power, and therefore the power block can operate longer producing more electricity. It is interesting to notice that the electricity yield (and hence, the capacity factor) increases non linearly with the solar multiple: it increases rapidly with the SM for small fields and more slowly with bigger fields. The explanation for this is that for a fixed storage capacity, increasing the solar field will initially make the steam turbine operate at full load for a longer period, but once the solar field is big enough, increasing even more the solar field will lead to moments where the storage is full and the turbine is working at full load, and hence some of the solar thermal power produced will be unused.

It is noteworthy that, for the case of no thermal storage, the annual net electricity production is significantly smaller than for a parabolic trough solar plant. For the smallest solar field ($SM = 1$), the annual net electricity yield of the plant with no storage is almost 60 $\%$ smaller than for a parabolic trough field of the same aperture area (Giostri et al. (2012)).This is due to the lower efficiency of the solar field of the LFR field compared to parabolic trough solar field.

The impact of the thermal storage in the capacity factor can be seen clearly in the solar plants with higher SM. It is not a linear relation: the impact of increasing the storage capacity is more important for lower storage capacities. The reason for this is that smaller storage capacities can be exploited fully more days a year (days with clear sky and high irradiation) than bigger, which will be partially used in many occasions.

4.3. Thermo-economic optimization

Based on the annual electricity production of the plants an economic study has been performed using different indicators: the Levelized Cost of Electricity and the Net Present Value.

The Levelized Cost of Electricity (LCOE, [c€/kWh_{e}]) is one of the most important indicators to compare different power plants. It measures the total costs over the energy yield, E_{ann}. The value of the LCOE depends on the investment and operation and maintenance (O&M) costs, $C_{O\&M}$, that can vary depending of the country and the level of development of the technique.

The LCOE has been calculated using eq. 18.

$$LCOE = \frac{C_{invest} \cdot (CRF + f_{ins,ann}) + C_{O\&M}}{E_{ann}} \tag{18}$$

where CRF is the capital recovery factor is defined as:

$$CRF = \frac{i_{rate}(1 + i_{rate})^n}{(1 + i_{rate})^n - 1} \tag{19}$$

The annual insurance cost, $f_{ins,ann}$, the debt interest rate, i_{rate} and the detailed investment costs, C_{invest}, used to calculate the LCOE, are shown in the table below:

Parameter	**Value**
Investment costs	
Solar field cost (€/m^2)	120[1]
Land cost (€/m^2)	2[2,3]
Thermal storage cost (€/kWh_{th})	65.65[4]
Power block cost (€/kW_{e})	700[3]
Construction, engineering and contingencies (%)	20[3]
—	—
Labour cost per employee and year (€/$year$)	48,000[5]
Number of employees (for plant operation)	30[3]
Number of employees (field maintenance), (empl/m^2)	$2 \cdot 10^{-5}$ [5]
O&M of investment per year (%)	1[2]
—	—
Annual insurance cost, $f_{ins,ann}$ (%)	1[2,3]
Lifetime (years), n	30[2]
Debt interest rate, i_{rate} (%)	8[2,3]

Table 5: Cost data used the economical analysis. Sources: [1] Rovira et al. (2016). [2] Montes et al. (2009a). [3]Montes et al. (2009b). [4] Prieto et al. (2018) [5] Morin et al. (2012).

Figure 6 shows the LCOE for the different solar and storage sizes. Each solid line corresponds to the evolution of the LCOE with the solar multiple for a different storage capacity. The dashed black thick line corresponds to the minimum LCOE at each solar multiple (with different storage capacities).

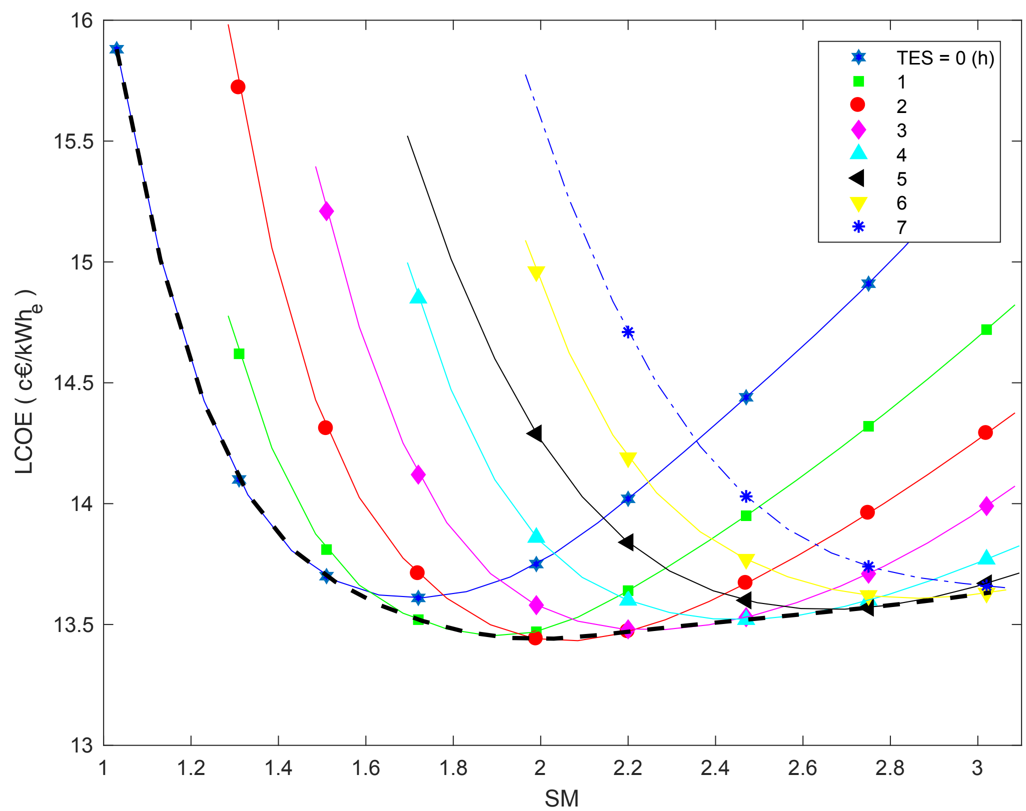

Figure 6: Influence of the storage size and solar multiple in the LCOE. Solid color lines represent power plants with different thermal storage capacity and dashed black thick line identifies the minimum LCOE of the Fresnel plants considered in the study.

For the case of no thermal storage (blue solid line with stars in fig. 6) the LCOE presents a minimum, similarly to what happens in parabolic plants (Montes et al. (2009b)). The LFR solar field has a lower efficiency than the PTC solar field, but its costs is smaller, and hence the optimum SM is higher for the LFR. The optimum solar multiple in the case of LFR technology is found at $SM = 1.72$ with a value of 13.61 c€/kWh$_e$, whereas Montes et al. (2009b) found the optimum SM for PTC plants was close to

1.2, and a LCOE of approximately 13.3 c€/kWh$_e$.

It can be noticed, that for the cases of LFR plants with storage, the LCOE reaches a minimum, similar to the cases of no-storage. For each solar multiple, the optimum storage size that reduces the LCOE varies from 0 h (for the smallest solar field) to 5 hours (for the largest solar field). Furthermore, it can be seen for all the lines (all storage sizes), and especially for the line representing the optimum plants (dashed black thick line), that the slope is bigger (in magnitude) for plants with SM smaller that the optimum than for solar plants with bigger SM. Hence, the solar field size plays a more important role for smaller LFR plants than for bigger ones, and increasing the solar field size over the optimum does not increase importantly the LCOE, whereas having a too small solar field increases notably the LCOE.

Regarding the thermal storage size, it can be seen that the higher is the solar multiple the larger is the thermal storage capacity that minimizes the LCOE. Or in other words, for LFR large solar field a high TES capacity is needed to ensure that the power block is working at full load during long periods of time and reduce the levelized cost of electricity. The optimum storage size (2 hours) is substancially smaller than when the heat transfer fluid is molten salts (15 hours according to Bacheller and Stieglitz (2017)), due to the high prices of the PCM storage compared with molten salts tanks.

It should be noted that the minimum LCOE is 13.44 c€/kWh$_e$, corresponding to the case of $SM = 1.99$ and 2 hours of TES.

On the other hand, the Total Net Present Value (TNPV) is a profit-based indicator that allows to calculate the internal rate of return. This cost-benefit analysis is employed commonly when analyzing the profitability of CSP power plants (Li et al., 2014; Kost et al., 2013) or improvements implemented to these plants (Okoye and Atikol, 2014; Rodríguez-Sánchez et al., 2014; Marugán-Cruz et al., 2015). Naturally this analysis strongly depends on the cost assumptions and on the markets incentives for these plants.

The Spanish average market price from 2000 to 2017 (excluding 2008, which was an atypical year due to the high price of the barrel of Brent crude oil that almost reached the 150 \$ in June) is 4.16 c€/kWh$_e$ (OMIE, 2017). The Spanish regulatory system, that was initially favorable to CSP development (BOE, 2007), has modified the remuneration scheme on several occasions increasing the investors risk. Under the current legislation, new renewable power plants will not receive any amount as remuneration on initial investment (BOE, 2014). This situation has led to no new installations of CSP plants in Spain since 2013. Due to the high investment costs, no CSP plant is cost competitive with traditional power plants and needs to be supported by feed-in tariffs or power-purchased agreements. However, for the calculation of TNPV, the average price of the remuneration for the current CSP plants in Spain since 2014 has been used: 29.557 c€/kWh$_e$ (CNMC, 2017). The TNPV has been calculated using the following equation:

$$TNPV = \sum_{k=1}^{n} \frac{B_k - C_k}{(1+\tau)^k} \tag{20}$$

where B_k is the annual revenue, C_k represents the annual expenses, τ is the discount rate (5.0%) and n is the service period (30 years). The revenue is calculated as the Annual net Electricity (see figure 5) times the remuneration price (29.557 c€/kWh). The expenses are the operation and maintenance costs, the investment costs and repayment of the loans (see eq. 21).

$$C_k = \left(IC - (k-1)\frac{IC}{RY} \right) \cdot r + \frac{IC}{RY} \tag{21}$$

where IC is the total investment costs, r is the interest rate of the loans (8%), RY is the prepayment period of the loans (10 years). The costs are detailed in table 5.

The internal rate of return, IRR, has been calculated using eq. 20, as the discount rate that makes the TNPV zero at the end of the project. For all the plants the IRR is larger than 100%, and that is why the incentives implemented by the Spanish governments led to the installation of CSP. All configurations presented in this paper would be profitable in the scenario presented in the paper (remuneration of 29.557 c€/kWh$_e$).

5. Conclusions

This paper presents a detailed analysis of the influence of solar field and energy storage size on the annual performance of direct steam generation linear Fresnel plants with integrated thermal energy storage. In the present study, solar-only power plants have been considered (no fossil hybridation). A model for the off-design performance of the solar field has been developed to simulate the annual behaviour of a linear Fresnel power plant. The power block performance, both at nominal and part load, has been evaluated. Based on the presented analysis the following conclusions have been drawn:

- The size of the solar field (solar multiple) and the thermal storage capacity have been optimized to obtain the minimum LCOE, based on the annual performance simulations. The optimum LFR 50 MW_e plant corresponds to a SM of 2 and TES of 2 hours with a LCOE of 13.44 c€/kWh_e. Despite of the lower efficiency of LFR, PTC and LFR plants present very similar values of LCOE.

- It has been found that increasing the solar multiple increases the energy yield, and that its effect on the annual net electricity (and the capacity factor) of the LFR power plants is more important for small size solar fields. Compared to PTC plants using synthetic oil, which are the most common CSP plants, the optimum solar multiple is larger for DSG linear Fresnel plants because of the smaller efficiency of the linear Fresnel reflectors.

- The relation between the thermal storage capacity and the annual net electricity is non linear: as the TES size increases, so does the annual net electricity, and the effect of increasing the size of the thermal storage is more important on LFR power plants with small storage.

- DSG linear Fresnel plants with high storage capacity have higher capacity factor, but larger LCOE due to the high costs of TES systems for direct steam generation. Hence, the size of the TES has to be kept relatively small, since otherwise the LCOE increases importantly.

Acknowledgements

The authors gratefully acknowledge the financial support given by the Spanish Ministerio de Economía y Competitividad and the European Regional Development Fund through the project ENE2015-69486- R (MINECO /FEDER, UE).The authors would like thank Felix Pérez-Cicala for his help with the partial-load code and his assistance with its modifications.

References

Abbas, R., Muñoz, J., Martínez-Val, J. M., 2012. Steady-state thermal analysis of an innovative receiver for linear Fresnel reflectors. Applied Energy 92, 503–515.

Al-Alili, A., Hwang, Y., Radermarcher, R., 2012. A high efficiency solar air conditioner using concentrating photovoltaic/thermal collectors. Applied Energy 93, 138–147.

Bacheller, C., Stieglitz, R., 2017. Design and optimisation of linear Fresnel power plants based on the direct molten salt concept. Solar Energy 152, 171–192.

Barlev, D., Vidu, R., Stroeve, P., 2011. Innovation in concentrated solar power. Solar Energy Materials and Solar Cells 95, 2703–2725.

Bellos, E., Tzivanidis, C., Papadopoulos, A., 2018. Daily, monthly and yearly performance of a linear Fresnel reflector. Solar Energy 173, 517–529.

BOE, 2007. RD 661/2007. A22846-22886. Official State Gazette (in Spanish). https://www.boe.es, accessed: 2018-10-09.

BOE, 2014. RD 413/2014. BOE-A-2014-6123. Official State Gazette (in Spanish). https://www.boe.es, accessed: 2018-10-09.

Burkholder, F., Kutscher, C., 2008. Heat Loss Testing of Schott's 2008 PTR70 Parabolic Trough Receiver. NREL Technical Report. NREL/TP-550-45633.

Cau, G., D., C., 2014. Use of parabolic trough solar collectors for solar refrigeration and air-conditioning applications. Energy Procedia 45, 101–110.

CNMC, 2017. National Commission on Markets and Competition (in spanish). https://www.cnmc.es/en/ambitos-de-actuacion/energia/liquidaciones-y-regimen-economico, accessed: 2018-10-19.

Desai, N. B., Bandyopadhyay, S., 2017. Line-focusing concentrating solar collector-based power plants: a review. Clean Technology Environmental Policy 19, 9–35.

Farjana, S. H., Huda, N., Parvez Mahmud, M., Saidur, R., 2018. Solar industrial process heating systems in operation – Current SHIP plants and future prospects in Australia. Renewable and Sustainable Energy Reviews 91, 409–419.

Feldhoff, J. F., Benítez, D., Eck, M., Riffelmann, K. J., 2010. Economic potential of solar thermal power plants with direct steam generation compared with HTF plants. Journal of Solar Energy Engineering 132, 041001–1–9.

Feldhoff, J. F., Schmitz, K., Eck, M., Schnatbaum-Laumann, L., Laing, D., Ortiz-Vives, F., Schulte-Fischedick, J., 2012. Comparative system analysis of direct steam generation and synthetic oil parabolic trough power plants with integrated thermal storage. Solar Energy 86, 520–530.

Gil, A., Medrano, M., I., M., Lázaro, A., Dolado, P., Zalba, B., Cabeza, L., 2010. State of the art on high temperature thermal energy storage for power generation. part 1-concepts, materials and modelization. Renewable and Sustainable Energy Reviews 14, 31–55.

Giostri, A., Binotti, M., Astolfi, M., Silva, P., Macchi, E., Manzolini, G., 2012. Comparison of different solar plants based on parabolic trough technology. Solar Energy 86, 1208–1221.

González-Roubaud, E., Pérez-Osorio, D., Prieto, C., 2017. Review of commercial thermal energy storage in concentrated solar power plants: Steam vs. molten salts. Renewable and Sustainable Energy Reviews 80, 133–148.

Grena, R., Tarquini, P., 2011. Solar linear Fresnel collector using molten salt nitrates as heat transfer fluid. Energy 36, 1048–1056.

Guo, J., Huai, X., Cheng, K., 2018. The comparative analysis on thermal storage systems for solar power with direct steam generation. Renewable Energy 115, 217–225.

Guédez, R., Topel, M., Conde, I., F., F., Caballa, I., Spelling, J., Hassar, Z., Pérez-Segarra, C., Laumer, B., 2016. A methodology for determining optimum solar power tower plant configurations and operating strategies to maximize profits based on hourly electricity market prices and tariffs. Journal of Solar Energy Engineering 138, 021006–1–12.

Industrial Solar, 2017. Linear fresnel collector lf-11. http://www.industrial-solar.de/en/products/fresnel-collector/, accessed: 2018-10-09.

Izquierdo, S., Montañés, C., Dopazo, C., Fueyo, N., 2010. Analysis of csp plants for the definition of energy policies: The influence on electricity cost of solar multiples, capacity factors and energy storage. Energy Policy 38, 6215–6221.

Johnson, M., Vogel, J., Hempel, M., Dengel, A., 2017. Design of high temperature thermal energy storage for high power levels. Sustainable Cities and Society 35, 758–763.

Johnson, M., Vogel, J., Hempel, M., Dengel, A., Seitz, M., Hachmann, B., 2015. High temperature latent heat thermal energy storage integration in a co-gen plant. Energy Procedia 73, 281–288.

Kolb, G. J., Clifford, H. K., Mancini, T. R., Gary, J. A., 2011. Power Tower Technology Roadmap and Cost Reduction Plan. Report No. SAND2011-2419, Alburquerque, NM, USA.

Kost, C., Flath, C. M., Möst, D., 2013. Concentrating solar power plant investment and operation decisions under different price and support mechanisms. Energy Policy 61, 238–248.

Kumar, K. R., Reddy, K. S., 2012. 4-E (energy–exergy–environmental–economic) analyses of line-focusing stand-alone concentrating solar power plants. Int J Low-Carbon Technol 7, 82–96.

Laing, D., Bauer, T., Breidenbach, N., Hachmann, B., Johnson, M., 2013. Development of high temperature phase-change-material storages. Applied Energy 109, 497–504.

Laing, D., Eck, M., Hempel, M., Steinmann, W. D., Meyer-Grünefeldt, M., Eickhoff, M., 2012. Analysis of operation test results of a high temperature phase change storage for parabolic trough power plants with direct steam generation. In: ASME 2012 6th Int. Conf. Energy Sustain. Parts A B. No. 273.

Li, J., Wu, Z., Zeng, K., Flamant, G., Ding, A., J., W., 2017. Safety and efficiency assessment of a solar-aided coal-fired power plant. Energy Conversion and Management 150, 714–724.

Li, W., Wei, P., Zhou, X., 2014. A cost-benefit analysis of power generation from commercial reinforced concrete solar chimney power plant. Energy Conversion and Management 79, 104–113.

Lippke, F., 1995. Simulation of the Part-Load Behaviour of a 30 MWe SEGS Plant. Report No. SAND95-1293, Alburquerque, NM, USA.

Lovegrove, K., Stein, W., 2012. Concentrating Solar Power Technology: Principles, Developments and Applications. Woodhead Publishing.

Luo, Y., Du, X., Yang, L., Xu, C., Amjad, M., 2017. Impacts of solar multiple on the performance of direct steam generation solar power tower plant with integrated thermal storage. Frontiers in Energy 11, 461–471.

Marugán-Cruz, C., Sánchez-Delgado, S., Rodríguez-Sánchez, M. R., M., V., D., S., 2015. District cooling network connected to a solar power tower. Applied Thermal Energy 79, 178–2015.

Mertins, M., 2008. Technische und wirtschaftliche Analyse von horizontal en Fresnel-Kollektoren. PhD Thesis.

Mills, D., 2004. Advances in solar thermal electricity technology. Solar Energy 76, 19–31.

Mills, D., Morrison, G. L., 2000. Compact lineal Fresnel reflector solar thermal power plants. Solar Energy 68, 263–283.

Mokhtar, G., Boussad, B., Noureddine, S., 2016. A linear Fresnel reflector as a solar system for heating water: Theoretical and experimental study. Case Studies in Thermal Engineering 8, 176–186.

Mokhtar, M., Ali, M. T., Bräuniger, S., Afshari, A., Sgouridis, S., Armstrong, P., M., C., 2010. Systematic comprehensive techno-economic assessment of solar cooling technologies using location-specific climate data. Applied Energy 87, 3766–3778.

Mokhtar, M., Berger, M., Zahler, C., Krüger, D., 2015. Direct steam generation for process heat using Fresnel collectors. Int. J. Therm. Eng. 10, 3–9.

Montes, M. J., Abánadez, A., Martínez-Val, 2009a. Performance of a direct steam generation solar thermal power plant as a function of the solar multiple. Solar Energy 83, 679–689.

Montes, M. J., Abánadez, A., Martínez-Val, J. M., Valdés, M., September 2009b. Solar multiple optimization for a solar-only thermal power plant, using oil as heat transfer fluid in the parabolic trough collectors. Solar Energy 83, 2165–2176.

Morin, G., Dersch, J., Platzer, W., Eck, M., Häberle, A., 2012. Comparison of Linear Fresnel and Parabolic Trough Collector power plants. Solar Energy 86, 1–12.

Novatec Solar, 2017. Concentrated Solar Power by Novatec Solar. http://www.novatecsolar.com/40-1-Download-Centre.html, accessed: 2018-10-09.

NREL, 2018. Linear Fresnel Reflector Projects. https://solarpaces.nrel.gov/by-technology/linear-fresnel-reflector, accessed: 2018-10-09.

Okoye, C., Atikol, U., 2014. A parametric study on the feasibility of solar chimney power plants in North Cyprus conditions. Energy Conversion and Management 80, 178–187.

OMIE, 2017. Market Results. `https://www.omie.es`, accessed: 2018-10-09.

Patnode, A. M., 2006. Simulation and Performance Evaluation of Parabolic Trough Solar Power Plants. PhD Thesis.

Petrakopoulou, F., Sánchez-Delgado, S., Marugán-Cruz, C., Santana, D., 2017. Improving the efficiency of gas turbine systems with volumetric solar receivers. Energy Conversion and Management 149, 579–592.

Pino, F. J., Caro, R., Rosa, F., Guerra, J., 2013. Experimental validation of an optical and thermal model of a linear Fresnel collector system. Applied Thermal Engineering 50, 1463–1471.

Polsky, M. P., 1982. Sliding pressure operation in combined cycles. In: Proceedings of the ASME. International Gas Turbine Conference and Exhibit. pp. 1–5.

Prieto, C., Rodríguez, A., Patiño, D., Cabeza, L. F., 2018. Thermal energy storage evaluation in direct steam generation plants. Solar Energy 159, 501–509.

Pulido-Iparraguirre, D., Valenzuela, L., Serrano-Aguilera, J. J., Fernandez-Garcia, A., 2019. Optimized design of a Linear Fresnel reflector for solar process heat applications. Renewable Energy 131, 1089–1106.

Pérez-Cicala, J., 2017. Rankine cycle modelling using the Spencer, Cotton and Cannon Method (in Spanish). Masters Thesis.

Qiu, Y., He, Y.-L., Cheng, Z.-D., Wang, K., 2015. Study on optical and thermal performance of a linear Fresnel solar reflector using molten salt as HTF with MCRT and FVM methods. Applied Energy 146, 162–173.

Rodríguez-Sánchez, M. R., Sánchez-González, A., Marugán-Cruz, C., Santana, D., 2014. Saving assessment using the PERS in solar power towers. Energy Conversion and Management 87, 810–819.

Rovira, A., Barbero, R., Montes, M. J., Abbas, R., Varela, F., 2016. Analysis and comparison of integrated solar combined cycles using parabolic troughs and linear Fresnel reflectors as concentrating systems. Applied Energy 162, 990–1000.

Schenk, H., Hirsch, T., Feldhoff, J. F., Wittmann, M., 2014. Energetic comparison of linear Fresnel and parabolic trough. Journal of Solar Energy Engineering 136, 041015–1–041015–15.

Schott, 2017. Schott ptr70 receivers. the 4th generation. http://www.schott.com/d/csp/370a8801-3271-4b2a-a3e6-c0b5c78b01ae/1.0/schott_ptr70_4th_generation_brochure.pdf, accessed: 2018-10-09.

Seitz, M., Johnson, M., Hïbner, S., 2017. Economic impact of latent heat thermal energy storage systems within direct steam generating solar thermal power plants with parabolic troughs. Energy Conversion and Management 143, 286–294.

Singh, P., Sarviya, R. M., Bhagoria, J., 2010. Thermal performance of linear Fresnel reflecting solar concentrator with trapezoidal cavity absorbers. Applied Energy 87, 541–550.

Spencer, R. C., Cotton, K. C., N., C. C., 1963. A method for predicting performance of steam generators:. 16,500 kw and larger. J. Eng. Power 4, 249–298.

SUNCNIM, 2017. Fresnel Suncnim Solar Steam Generator. https://www.suncnim.com/sites/default/files/2017-06/SUNCNIM\%20leaflet\%20EOR.pdf, accessed: 2018-10-09.

Velázquez, N., García-Valladares, O., Sauceda, D., Beltrán, R., 2010. Numerical simulation of a Linear Fresnel Reflector Concentrator used as direct generator in a Solar-GAX cycle. Energy Conversion and Management 51, 434–445.

Wagner, M. J., 2012. Results and Comparison from the SAM Linear Fresnel Technology Performance Model. NREL/CP-5500-54758 -.

Wagner, M. J., Zhu, G., 2012. A direct steam linear Fresnel performance model for NREL's System Advisory Model. In: Svartholm, N. (Ed.), Proceedings of the ASME 2012 6th International Conference on Energy Sustainability and Fuel Cell Science, Engineering and Technology Conference. pp. 1–8.

Wang, F., Zhao, J., Li, J., Deng, S., Yan, J., 2017. Preliminary experimental study of post-combustion carbon capture integrated with solar thermal collectors. Applied Energy 185, 1471–1480.

Yang, Y., Yan, Q., Zhai, R., Kouzani, A., Hu, E., 2011. An efficient way to use medium-or-low temperature solar heat for power generation e integration into conventional power plant. Applied Thermal Energy 31, 157–162.

Zhu, G., Wendelin, T., Wagner, M. J., Kutscher, C., 2014. History, current state and future of linear Fresnel concentrating solar collectors. Solar Energy 103, 639–652.